Generalized Modal Decoupling Control for Active Magnetic Bearings

Pascal Zeugin
Mecos AG
Zurich, Switzerland
pascal.zeugin@mecos.com

Beat Aeschlimann
ZHAW
Winterthur, Switzerland
aesc@zhaw.ch

Michael Hubatka
OST
Rapperswil, Switzerland
michael.hubatka@ost.ch

***Abstract*—Control design for unstable, uncertain, and highly coupled MIMO (Multiple Input and Multiple Output) systems such as AMB (Active Magnetic Bearing) systems is extremely challenging and requires sophisticated synthesis strategies. While postmodern control methods such as μ-synthesis may be able to solve such problems, they require an accurate mathematical model of the system and specialized software tools for the controller synthesis. The resulting control algorithms are typically of excessively high order and therefore computationally demanding and challenging to implement.**

In contrast, the control culture of the magnetic bearing engineering community also offers classical, essentially single-input, single-output (SISO) methods to produce reliable and robust solutions to a wide variety of control problems. One well-known approach is translational-tilting modal-transformation control. However, this approach is limited in cases where the first bending mode is close to the desired closed-loop rigid body modes.

This paper describes an approach for hand-synthesized, generalized modal decoupling control design for magnetically levitated rotors. The basic idea of this method is to use the singular value decomposition (SVD) to transform the decentralized inputs and outputs into generalized modal coordinates. This greatly simplifies the design of the controller, which in turn allows for much more sophisticated rotor dynamic designs by independently controlling the decoupled mode. This can be viewed as a generalization of the known decoupling transformations.

The transformation works with both model- and measurement-based frequency response functions, in contrast to the known approaches in the literature, and is shown to excel where common classical control methods fail. Results and comparisons are demonstrated by an experimental evaluation of the frequency domain control performance of a supercritical gas turbine.

***Index Terms*—MIMO-control, uncertain systems, robust control, AMB-system, rotor dynamics, Singular Value Decomposition**

I. Introduction

Magnetic bearing systems for rotating machinery are a prime example of robust MIMO control because they inherently involve many conflicting performance objectives. The system to be controlled exhibits significant variations in plant dynamics over the operating speed range, which is commonly referred to as a plant with high uncertainty. Essentially, this is the archetypal challenge for robust control techniques such as μ-synthesis, which, in contrast to classical and modern control methods, explicitly deals with uncertainty [1]. However, there are several requirements that must be met, such as

- Availability of a detailed plant model with uncertainty description
- Proprietary, sophisticated software tools
- Well-trained control engineers with a strong mathematical background
- Computing power for controller synthesis
- Numerically robust and efficient controller implementation.

Despite the fact that model-based postmodern robust control techniques are exceptionally powerful, if one or more of these requirements are not met, these methods cannot be applied. On the other hand, there are the proven classical control methods that have reliably produced robust solutions to a wide variety of control problems for decades.

The simplest and most intuitive way to tackle the control of an active magnetic bearing system is the so-called decentralized control, where each sensor feeds back to the actuator in the same degree of freedom [2]. However, in some systems this introduces significant off-diagonal coupling terms in the resulting transfer matrix, which in turn makes the task of control design very difficult. Zhang et al. introduced a method of modal decoupling control for systems with strong gyroscopic effects [3], where the big advantage is that the translational and tilting modes can be influenced almost independently of each other in different control channels. In other words, the speed-dependent gyroscopic effects of nutation and precession occur only in the tilt-mode control channel, where they are relatively easy to handle.

A similar technique is shown by Hutterer, Hofer, and Schrödl in [4]. However, these approaches are limited because they fail when the first bending mode is close to the closed-loop rigid body modes. In summary, no successful approaches to decoupling modes other than rigid body modes have been reported.

The following sections present the main ideas of the new method in the order of a typical engineer's workflow. The workflow starts by analyzing and highlighting the limitations of existing decoupling methods. This is followed by a brief summary of the mathematical foundations of the new method and its physical implications with respect to rotor dynamics. Finally, a case study demonstrates the application of the technique and evaluates its control performance using a real-world example.

II. Limitations of Translational-Tilting Control

Well-known decoupling methods such as translational-tilting control implement MIMO control while preserving the ability to interpret feedback parameters as physical quantities in a SISO-like manner, similar to local feedback. This control structure exploits the physical effect that the parallel and conical modes of the rigid body system can be decoupled using static transformation matrices, as shown in the Figure 1 for a plane through x and z coordinates (xz-plane). By transforming the controller input signals $\{x_{seA}, x_{seB}\}$ with T_{in} so that the parallel and conical modes can be detected separately, these modes can also be controlled separately. The controller output signals, which physically correspond to the torque τ and the concentrated force f_x with respect to the rotor center of gravity S, then only need to be transformed into suitable forces $\{f_{xA}, f_{xB}\}$ in the bearing planes A and B with T_{out} [5].

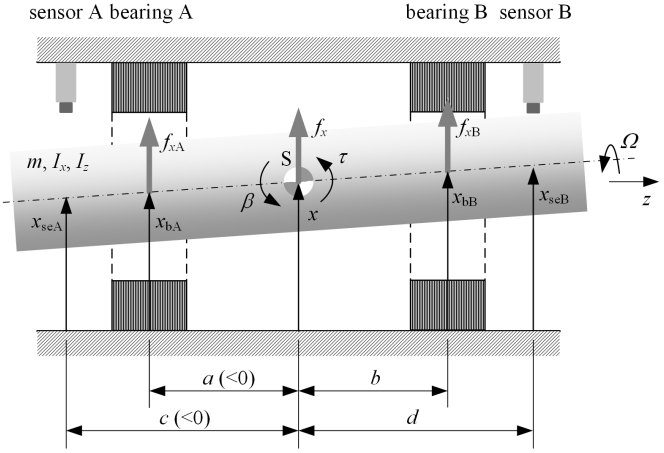

Fig. 1: Rigid rotor with bearing magnets and sensors as well as displacements and forces [5].

In this way, modal control of the rigid body modes is achieved. Figure 2 shows the corresponding control architecture.

To stabilize the rigid body modes in an AMB system, the controllers $G_{p/c,x/y}$ need sufficient positive phase (PD control, lead element) around the crossover frequency of the open-loop system. This results in high controller gains at higher frequencies, which is undesirable due to noise amplification and a destabilizing effect on the flexible modes. To overcome these problems, the controller features a low-pass, i.e. roll-off filter.

In a typical rotor design, the first flexible mode is well separated from the rigid body modes. If the desired closed loop bandwidth is around 50 Hz and the flexible mode is above 500 Hz, it is possible to use a steep roll-off to avoid excitation of the bending mode. If the bending mode is below 500 Hz, using a roll-off will compromise the positive phase to stabilize the rigid body mode. Moreover, this may not be admissible for all rotor designs as this procedure may violate the requirements for amplification factor and separation margin of the mode,

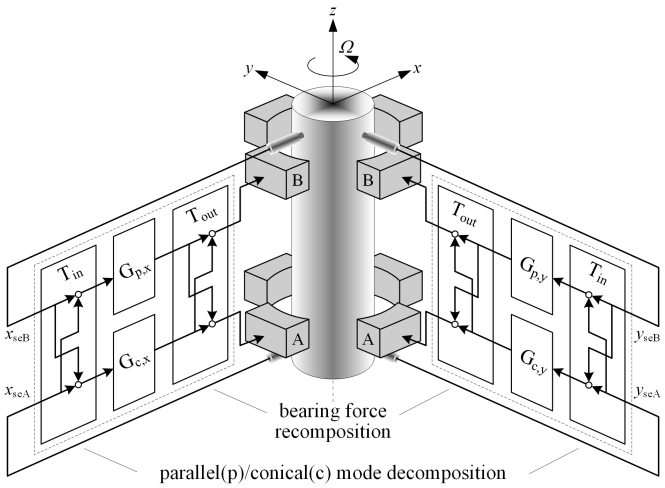

Fig. 2: Feedback structure for decoupled control of parallel and conical modes [5].

which are essentially designed to ensure that the rotor does not operate close to a ligthly-damped critical speed [6]. A possible, but theoretical solution is to use a positive phase in the controller to actively dampen the bending mode. This however results in even more gain in the controller, more noise amplification, potential actuator saturation, and excitation of other bending modes.

This means that the translational-tilting control architecture fails in applications where the first bending mode is too close to the rigid body modes.

A more sophisticated approach would be to separate the bending mode into a dedicated control channel. In the other control channel, the bending mode should be neither controllable nor observable.

III. Plant Model

The general plant model is represented by a small gas turbine with a maximum continous speed (MCS) of 35000 rpm. The rotor model G_p comprises 95 beam elements for the shaft and 4 lumped masses at the corresponding nodes to model the impellers. Before building up the complete system model, the rotor model is exported as mass, gyroscopic and stiffness matrices (MGK matrix form) and transformed into modal coordinates. This is important to model the rotor's speed-dependency resulting from its gyroscopic properties. Apart from the rotor, the full system model includes the actuator properties, amplifier dynamics, computational delay, negative stiffness of the motor and sensor dynamics. There are four force input stations $f = [f_{\text{A}x}, f_{\text{A}y}, f_{\text{B}x}, f_{\text{B}y}]^T$ at the locations of the magnetic bearings and four displacement output stations $r = [r_{\text{A}x}, r_{\text{A}y}, r_{\text{B}x}, r_{\text{B}y}]^T$ at the locations of the radial sensors. This is visualized in Figure 3, where the rotor and its modal analysis is shown.

The first flexible mode is at 226 Hz at standstill and the corresponding forward mode is crossed at around 270 rps. This

needs a special unbalance force counteracting control (UFCC) [9] algorithm, which is not part of this paper.

The dynamics of the rotor is modeled as a transfer function matrix $G_p(j\omega)$

$$r(\omega) = G_p(j\omega)f(\omega). \tag{1}$$

The bode magnitude plots are shown in figure 9.

IV. Generalized Modal Decoupling Control

To achieve generalized modal decoupling control, Singular Value Decomposition (SVD) is particularly useful because of its close relationship to signal amplification in systems. It is extremely important to have a thorough understanding of the SVD, so the following section is intended to be a concise summary of its mathematical foundations and physical implications with respect to rotor dynamics. Despite the fact that all of this theory is readily available in the literature, an effort has been made here to gather the best information and present it in a way that makes it accessible to the reader.

Let's start with induced matrix norms. Consider the equation

$$r = Gf. \tag{2}$$

If $f \in \mathbb{C}^m$ is the input vector and $r \in \mathbb{C}^p$ the output vector, then $\|r\|_2/\|f\|_2$ is said to be the "amplification" or "gain" of the constant complex matrix $G \in \mathbb{C}^{p\times m}$. The maximum gain for all possible input directions is of special interest and is given by the *induced norm* defined as

$$\|G\|_2 := \max_{f\neq 0} \frac{\|r\|_2}{\|f\|_2} = \max_{f\neq 0} \frac{\|Gf\|_2}{\|f\|_2}. \tag{3}$$

That is, the induced 2-norm gives the largest possible amplification of the constant matrix G. Therefore we need to find the direction of the vector f that maximizes the ratio $||r||_2/||f||_2$, which is a constrained optimization problem, namely finding

$$\max_{\|f\|_2^2=1} \|r\|_2^2. \tag{4}$$

Applying the method of Lagrange multipliers, to seek the critical points for the functional

$$\mathcal{L}(f,\lambda) = r^T r - \lambda\left(f^T f - 1\right) = 0 \tag{5}$$

$$= f^T G^T G f - \lambda\left(f^T f - 1\right) = 0. \tag{6}$$

Differentiating $\mathcal{L}$ with respect to f and λ yields

$$\frac{\partial \mathcal{L}}{\partial f} = 2\left(G^T G f - \lambda f\right) = 0 \tag{7}$$

$$\frac{\partial \mathcal{L}}{\partial \lambda} = f^T f - 1 = 0. \tag{8}$$

The stationary point satisfies the eigenvalue problem

$$G^T G f = \lambda f. \tag{9}$$

The eigenvalues λ of $G^T G$, subsequently referred to as σ_i^2, are strictly non-negative because $G^T G$ is a symmetric matrix. The positive roots σ_i are the so-called *singular values* of G. The largest of these singular values is the maximum amplification possible for the matrix G and is therefore $\|G\|_2$.

The normalized eigenvectors of $G^T G$ are v_i. Because $G^T G$ is symmetric, these eigenvectors are all perpendicular to each other and form a unitary matrix $V = [v_1\ v_2\ \ldots\ v_m]$ with the property $V^{-1} = V^H$.

Defining the normalized vectors

$$u_j = \frac{Gv_j}{\|Gv_j\|_2} = \frac{1}{\sigma_j} G v_j, \tag{10}$$

it can be shown that $U = [u_1\ u_2\ \ldots\ u_p]$ is also a unitary matrix with $U^{-1} = U^H$. Together with the matrix Σ, which is a diagonal matrix containing the non-zero, positive singular values σ_i. These are arranged in descending order along the diagonal, i.e

$$\sigma_1 \geq \sigma_2 \geq \ldots \sigma_m. \tag{11}$$

The SVD can be written as

$$GV = U\Sigma \tag{12}$$

or in the matrix factorization form

$$G = U\Sigma V^H. \tag{13}$$

In the two-dimensional space, the singular values have a nice graphical interpretation. Consider the matrix

$$G = \begin{pmatrix} 1.5 & 0 \\ -1.1 & 1.1 \end{pmatrix}.$$

The objective is to find the direction of the vector f, given $\|f\|_2 = 1$, which maximizes $\|Gf\|_2$. The norm constraint on f implies that f lies on the unit circle, like shown in figure 4. As the vector f is moved on the unit circle, $r = Gf$ describes an ellipse. To ensure SVD nomenclature consistency, v_1 corresponds to the direction of f with the maximum gain σ_1, whereas v_2 is referred to as the direction of f associated with the minimum gain σ_2.

The length of major and minor axes of this ellipse are the singular values σ_1 and σ_2 of the matrix G, respectively. To put it simply, out of all possible input directions the input vector v_1 creates the largest possible response in the direction of u_1.

This holds also if $G(j\omega)$ is a frequency depending matrix. For every fixed frequency ω there exist a SVD

$$G(j\omega) = U(j\omega)\Sigma(j\omega)V^H(j\omega). \tag{14}$$

That is, if G is frequency dependent, the singular values and singular vectors of the system will also have frequency dependence.

There is a nice physical interpretation of the SVD for a rotor model. Taking the model from section III evaluated at MCS and augmenting it by other force input stations at the beginning of the shaft, at the center of gravity and at the end of the shaft yields the following force vector

$$f_{\text{aug}} = \begin{bmatrix} f_{\text{beg},x} \\ f_{\text{beg},y} \\ f_{\text{cog},x} \\ f_{\text{cog},y} \\ f_{\text{end},x} \\ f_{\text{end},y} \end{bmatrix}.$$

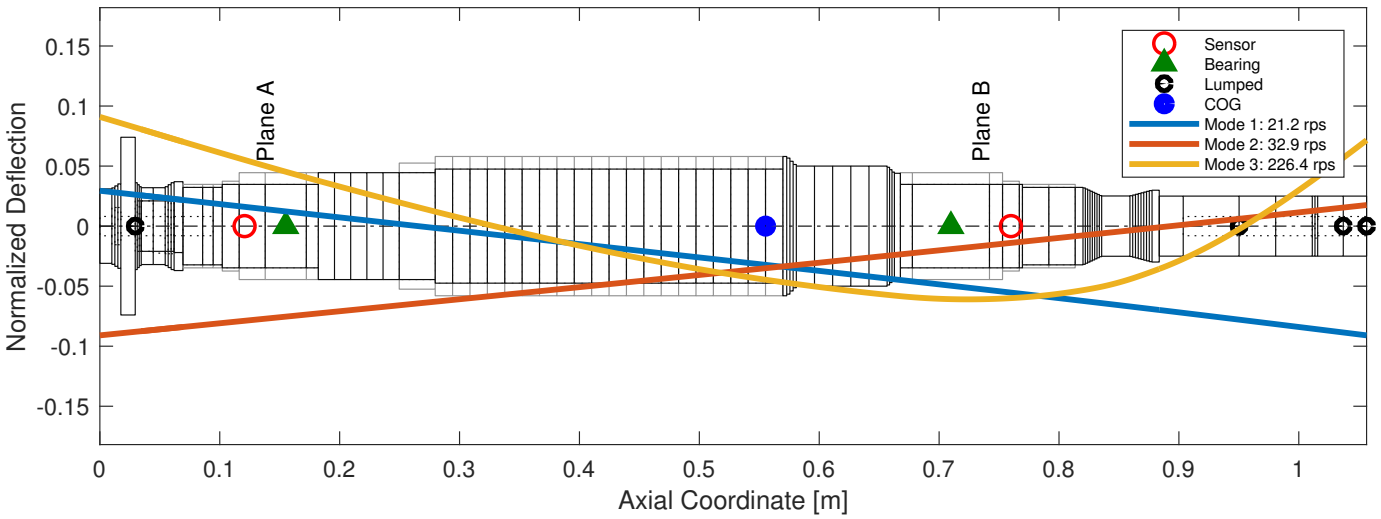

Fig. 3: Bending mode shapes of the corresponding natural frequency of the rotor. Both natural frequency and bending mode shape were calculated with a low bearing stiffness of $1 \cdot 10^6$ N/m to simulate free-free conditions.

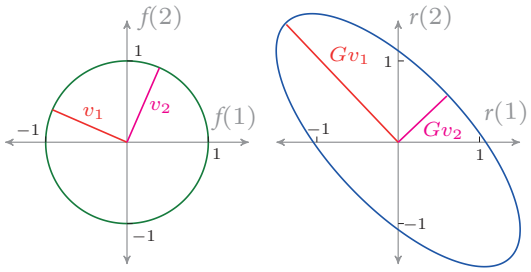

Fig. 4: Graphical interpretation of the singular value decomposition: The input f ($\|f\|_2 = 1$) is plotted on the left side, whereas the output $r = Gf$ is plotted on the right side

Such input forces are typical to excite the first bending mode [6]. Similarly, radial sensors are assumed to exist at every of the 95 nodes of the model.

$$r_{\text{aug}} = \begin{bmatrix} r_{\text{node1},x} \\ r_{\text{node1},y} \\ \vdots \\ r_{\text{node95},x} \\ r_{\text{node95},y} \end{bmatrix}.$$

This is expressed by the augmented plant transfer matrix

$$r_{\text{aug}}(\omega) = G_{\text{aug}}(j\omega) f_{\text{aug}}(\omega).$$

Now if the plant transfer matrix is evaluated at its natural frequency, i.e. the first bending eigenfrequency $G_{\text{aug}}(j\omega_n)$, a complex valued matrix G is obtained. Applying the SVD yields a complex left singular vector $u_1 = [u_{\text{node1},x}, u_{\text{node1},y}, \dots]^T$ which can be visualized by plotting the real and imaginary parts of its x- and y-elements, respectively, against the axial coordinates of the nodes (see Figure 5). Comparing Figure 5 with the mode shapes in 3 reveals that u_1 corresponds to the eigenshape of the first bending mode.

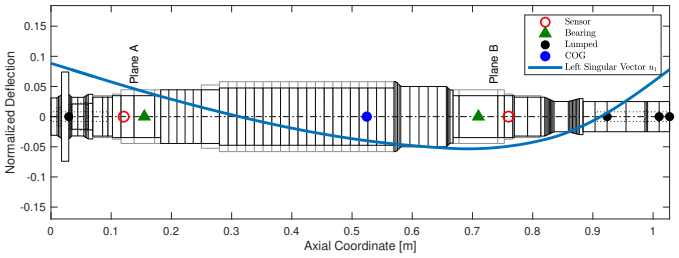

Fig. 5: Physical interpretation left singular vector u_1 of $G = G_{\text{aug}}(j\omega_n)$

Similarly, the right singular vector $v_1 \in \mathbb{C}^{2\cdot 3}$ can be thought of as some force distribution like unbalance along the rotor [7]. Out of all possible input directions, the force distribution which leads to maximum excitement of the rotor is where the force acting on the rotor's center of gravity is 180° out of phase with respect to forces at the rotor ends. Naturally, this will result in the largest possible response, which is exactly the bending mode as can be seen in Figure 6, where again the real and imaginary parts of the x- and y-elements of the singular vector is plotted against the respective axial node coordinates.

After resetting the displacement output stations and force input stations of the general plant model to the four locations of the radial sensors and magnetic bearings, respectively, the generalized modal decoupling control transformations can be found by examination of the left and right singular vectors u_1 and v_1, of the SVD of $G = G_p(j\omega_n)$, where ω_n denotes the frequency of the mode to be decoupled.

If $f \in \mathbb{R}^m$ and $r \in \mathbb{R}^p$, the transformation matrices to be found are represented by $T_{\text{U}} \in \mathbb{R}^{p\times p}, T_{\text{V}} \in \mathbb{R}^{m\times m}$. However, there is no loss of generality in assuming $m = 4$ and $p = 4$, as in the general plant model G_p. Now to create the new output vector which separates the natural frequency ω_n from its complement or null space, a transformation matrix T_{U}

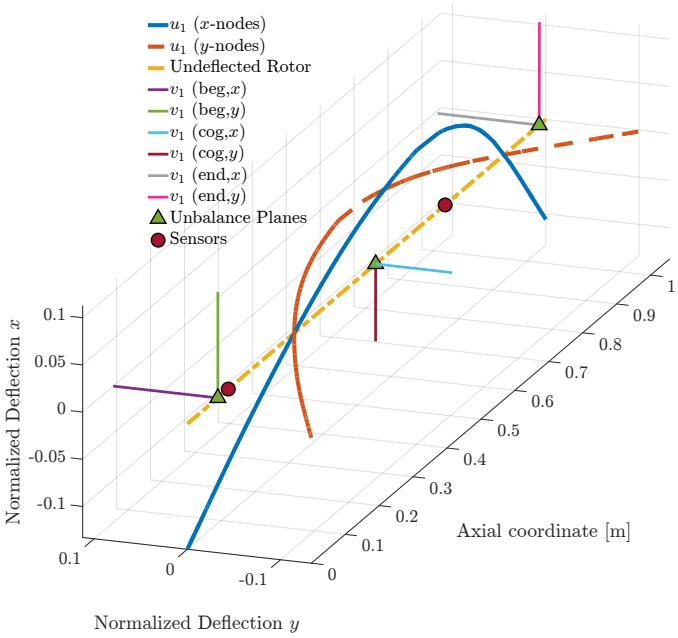

Fig. 6: Physical interpretation right singular vector v_1 of $G = G_{\text{aug}}(j\omega_n)$ and the resulting left singular vector u_1. Note that at resonance, the unbalance force and displacement are 90° out of phase.

which satisfies

$$\begin{bmatrix} r_{\text{mode},x} \\ r_{\text{mode},y} \\ \overline{r}_{\text{mode},x} \\ \overline{r}_{\text{mode},y} \end{bmatrix} = T_{\text{U}} \begin{bmatrix} r_{\text{A}x} \\ r_{\text{A}y} \\ r_{\text{B}x} \\ r_{\text{B}y} \end{bmatrix}. \tag{15}$$

needs to be found. $r_{\text{mode},x/y}$ are the transformed control input channels that contain the desired mode shape, and $\overline{r}_{\text{mode},x/y}$ are the transformed control channels that do not observe it.

Given that $u_1 = [u_{\text{A}x}, u_{\text{A}y}, u_{\text{B}x}, u_{\text{B}y}]^T$, it holds that the matrix from (16) satisfies (15)

$$\begin{aligned} u_{\text{ref},j} &= \frac{u_{\text{A}j}}{\|u_{\text{A}j}\|}, \; j \in \{x, y\} \\ \hat{T} &= \begin{bmatrix} u_{\text{A}x} \cdot u_{\text{ref},x} & 0 & u_{\text{B}x} \cdot u_{\text{ref},x} & 0 \\ 0 & u_{\text{A}y} \cdot u_{\text{ref},y} & 0 & u_{\text{B}y} \cdot u_{\text{ref},y} \end{bmatrix} \\ T_{\text{U}} &= \begin{bmatrix} \text{Re}\left(\hat{T}\right) \\ \ker\left(\text{Re}\left(\hat{T}\right)\right) \end{bmatrix} \end{aligned} \tag{16}$$

where $\ker(.)$ is the kernel or null space of a matrix. The main idea behind converting complex values in u_1 to real values in T_{U} is to generate real frames that are aligned as closely as possible to the given complex frames. This can be done with the ALIGN algorithm of Kouvaritakis [8]. However here, for ease of understanding, the idea and the corresponding algorithm is outlined using the dot product. Since the transformation matrix must be real-valued, the complex-valued entries of the singular vectors must be interpreted accordingly. By treating the first entry of the singular vector as the normalized reference vector in the complex plane, all entries can be aligned to this vector via the dot product.

Figure 7 graphically illustrates the entries of the left singular vector u_1 of $G = G_p(j\omega_n)$, which represent the rotor deflection of the bending mode shape at the sensor locations.

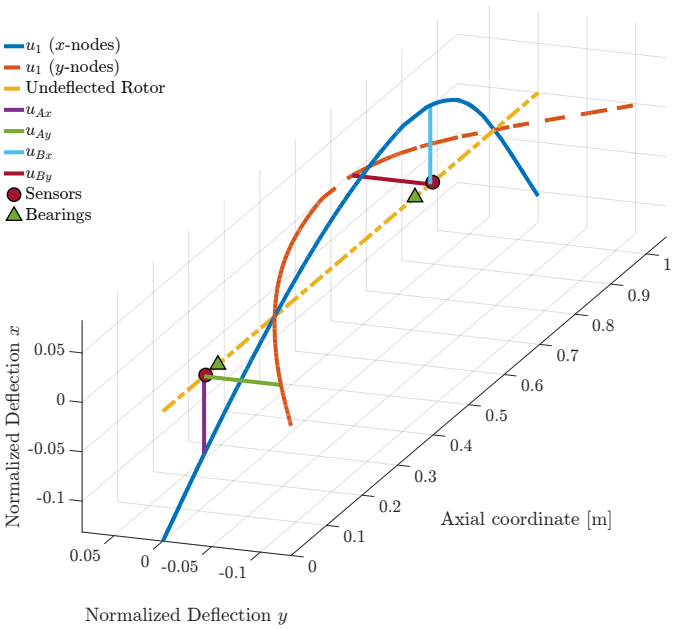

Fig. 7: Physical interpretation left singular vector u_1 of $G = G_p(j\omega_n)$

Similarly, given $v_1 = [v_{\text{A}x}, v_{\text{A}y}, v_{\text{B}x}, v_{\text{B}y}]^T$ a new input vector which directly influences the targeted mode shape and the corresponding complement or null space is found by (17) and (18), respectively.

$$\begin{bmatrix} f_{\text{mode},x} \\ f_{\text{mode},y} \\ \overline{f}_{\text{mode},x} \\ \overline{f}_{\text{mode},y} \end{bmatrix} = T_{\text{V}} \begin{bmatrix} f_{\text{A}x} \\ f_{\text{A}y} \\ f_{\text{B}x} \\ f_{\text{B}y} \end{bmatrix} \tag{17}$$

$$\begin{aligned} v_{\text{ref},j} &= \frac{v_{\text{A}j}}{\|v_{\text{A}j}\|}, \; j \in \{x, y\} \\ \tilde{T} &= \begin{bmatrix} v_{\text{A}x} \cdot v_{\text{ref},x} & 0 & v_{\text{B}x} \cdot v_{\text{ref},x} & 0 \\ 0 & v_{\text{A}y} \cdot v_{\text{ref},y} & 0 & v_{\text{B}y} \cdot v_{\text{ref},y} \end{bmatrix} \\ T_{\text{V}} &= \begin{bmatrix} \text{Re}\left(\tilde{T}\right) \\ \ker\left(\text{Re}\left(\tilde{T}\right)\right) \end{bmatrix}^T \end{aligned} \tag{18}$$

Figure 8 graphically illustrates the entries of the right singular vector v_1 of $G = G_p(j\omega_n)$ representing the input forces of the magnetic bearings which lead to the maximum excitement of the rotor. This algorithm may be generalised for a setup with many control planes, which allows to decouple multiple modes (see Equation 20). The letters A to Z represent the control planes and n denotes the number of mode frequencies

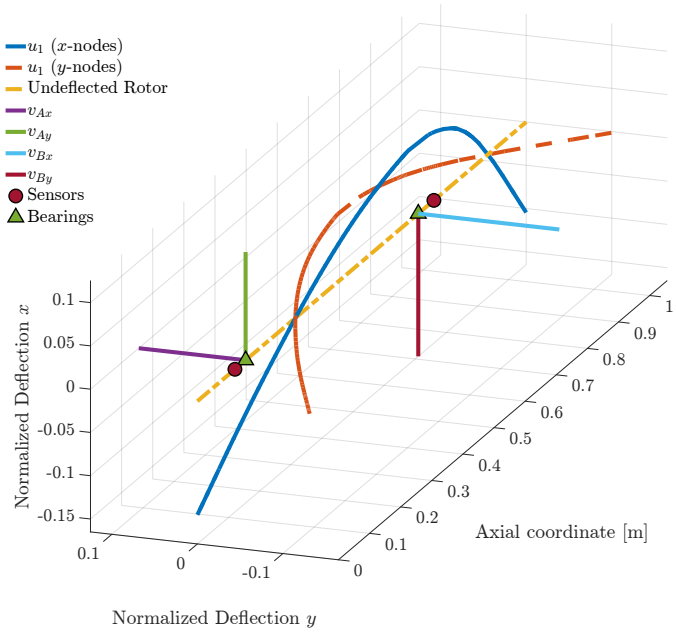

Fig. 8: Physical interpretation left singular vector v_1 of $G = G_p(j\omega_n)$. Note that at resonance, the unbalance force and displacement are 90° out of phase.

to be decoupled. In other words, the transformation matrix essentially consists of the blocks $T_{i,k} \in \mathbb{R}^{2\times 2}$, nicely stacked upon each other, where $i \in \{\mathrm{A}, \ldots, \mathrm{Z}\}$ and $i \in \{1, \ldots, n\}$. The input transformation T_V is obtained analogously when the left singular vector u is swapped with the right singular vector v.

V. Experimental Results

In this section the results achieved by the introduced decoupling control technique are investigated. The plant that is subject to this case study is a small gas turbine. The maximum continous speed (MCS) of the machine is 35000 rpm (583 rps) thus representing a supercritical application (MCS is above the the first flexible bending mode frequency). The model of the rotor borne by magnetic bearings is given in section IV. Its frequency response at standstill and maximum continous speed, respectively, can be found in the Bode plot in Figure 9 shown in blue.

In this section this model is used to design a hand-synthesized position controller, which meets the generally known and obvious objectives such as a sufficient stability margin and an adequate handling of external loads. It is vitally important to emphasize that the craftsmanship and optimization of hand-synthesized controllers is generally referred to as loop shaping[1] and is largely considered an art for systems with this level of complexity. As a result, the assessment of optimality of such controllers is non-trivial. However, the most straightforward and intuitive approach for designing a controller is to attempt to make the AMB act like conventional mechanical bearings at the actuator locations, that is, feedback control is being performed locally for each bearing unit and separately for each bearing axis. However, this approach, often referred to as decentralized control, over-simplifies the problem and must be adapted and extended for realistic rotor systems. Applying the Tilting-Translational coordinate transformation results in the brown frequency domain characteristics shown in Figure 9. It is not hard to see that the transformed plant features little to no benefits over the decentralized plant as the cross-coupling terms are still substantial and there is no useful mode separation. The golden transfer function is obtained by applying the generalized modal decoupling control transformation proposed in this paper, where the plant transfer matrix is evaluated at the first bending eigenfrequency (see Figure 3). The critical frequency is detected separately and can therefore be controlled separately, which greatly facilitates the control design. The design of a controller that meets the robustness and performance criteria of generalized modal decoupling control plant $G_{p,gmd}$ is fairly easy whereas the design that targets the tilting-translational control plant $G_{p,tt}$ is quite tedious and unable to meet the necessary performance criteria. This generally results in a conservative controller being unable to keep the rotor in position, i.e. centered under rotation. The position controller of the magnetic bearings must be able to maintain stability and performance under the influence of all plant uncertainties such as the splitting of eigenfrequencies due to gyroscopy, changes in suction pressure and gas composition to name a few. The ISO standard 14839 addresses this robustness issue and imposes limits on the peak value of the output sensitivity function $S_e = (I + L)^{-1}$. The standard recommends that the diagonal elements of S_e have a peak value below 3 for newly commissioned machines. However, this does not guarantee high performance of the closed-loop, i.e. small rotor orbits, good disturbance rejection, therefore other criteria must be introduced. Here the dynamic compliance G_f is used which is the relation between rotor displacement and external force[2]. Obviously, G_f must be as low as possible for all frequencies. Unlike the specification of S_e, there is no absolute upper limit for the compliance since it is dependent on the range of bearing force. As a result, the design goals can be summarized as follows:

- $\|S_e(i,i,j\omega)\|_\infty \leq 3,\ i \in \{1,\ldots,4\}$
- $\|G_f(j\omega)\|_\infty \leq \epsilon,\ \epsilon$ as small as possible

Now the controller design can be divided into the following steps.

- Due to the decoupling properties of the proposed transformation, the off-diagonal elements can be neglected.
- Due to rotor symmetry, only two SISO controllers must to be designed for the four diagonal elements of the transformed plant $G_{p,gmd}$.
- The controller is designed in order to robustly stabilize the plant, that is, fulfilling the generalized Nyquist

[1]This classical approach aims to shape the magnitude of the open-loop function $L(j\omega) = G_pG_c$, where G_c is the feedback controller to be designed and G_p is the plant.

[2]Dynamic compliance refers here to $G_f(j\omega) = G_p(j\omega)S_u(j\omega)$, where $S_u(j\omega)$ is the sensitivity function at the plant input.

$$u_{\mathrm{ref},j}(\omega) = \frac{u_{\mathrm{A}j}(\omega)}{\|u_{\mathrm{A}j}(\omega)\|},\ j \in \{x, y\} \tag{19}$$

$$T_{\mathrm{U}} = \begin{matrix} T_{i,k}^{2\times 2}\left\{\vphantom{\begin{matrix}a\\b\\c\\d\end{matrix}}\right. \\ \\ \\ \\ \\ \end{matrix} \begin{bmatrix} u_{\mathrm{A}x}(\omega_1)\cdot v_{\mathrm{ref},x}(\omega_1) & 0 & \cdots & u_{\mathrm{Z}x}(\omega_1)\cdot v_{\mathrm{ref},x}(\omega_1) & 0 \\ 0 & u_{\mathrm{A}y}(\omega_1)\cdot v_{\mathrm{ref},y}(\omega_1) & \cdots & 0 & u_{\mathrm{Z}y}(\omega_1)\cdot v_{\mathrm{ref},y}(\omega_1) \\ \vdots & \vdots & \ddots & \vdots & \vdots \\ u_{\mathrm{A}x}(\omega_n)\cdot v_{\mathrm{ref},x}(\omega_n) & 0 & \cdots & u_{\mathrm{Z}x}(\omega_n)\cdot v_{\mathrm{ref},x}(\omega_n) & 0 \\ 0 & u_{\mathrm{A}y}(\omega_n)\cdot v_{\mathrm{ref},y}(\omega_n) & \cdots & 0 & u_{\mathrm{Z}y}(\omega_n)\cdot v_{\mathrm{ref},y}(\omega_n) \\ \multicolumn{5}{c}{\ker\left(\mathrm{Re}\left(\tilde{T}\right)\right)} \end{bmatrix} \left.\vphantom{\begin{matrix}a\\b\\c\\d\end{matrix}}\right\}\tilde{T} \tag{20}$$

criterion for any plant in the set of transfer functions represented by uncertainty.

- Ensure that the design goals are met for any plant in the set of transfer functions represented by uncertainty.

Figure 10a and 10b show the controller which meets the design goals, in the centralized and decentralized coordinate system, respectively. During the machine commissioning, it was gradually accelerated to reach its maximum continuous speed. At various rotational speeds, relevant control signals were measured, and frequency domain measurements of the control plant and sensitivity S_e were conducted. This exercise ensured the stability of the control system at any rotational speed. In order to deal with umodeled dynamics, adjustments were made to further enhance the controller by augmenting it with numerous tricks such as notch and phase bump filters. Figure 11 shows the measured sensitivity functions S_e at standstill and at MCS. Evidently, the peak values of all diagonal elements at both rotation speeds are below 3, which implies that the closed-loop exhibits excellent robustness against plant uncertainties and falls into zone A, according to ISO 14839 [9].

VI. Conclusion

In this paper a generalized modal decoupling control method has been proposed, which essentially is able to split up the system into modal parts and its null space via coordinate transformation. The functionality of this transformation was proved by experiments on a supercritically operated small gas turbine. The transformation coordinate system rendered the task of control design substantially easier because it achieves true mode separation. This allows to stabilize the first bending mode over a great frequency range without compromising the other flexible modes on the modal channel, whereas the requirement to actively stabilize any flexible modes is completely eliminated on the complementary channel. Essentially, the proposed method is a generalisation and improvement of existing decoupling methods such as tilting-translational control, therefore it is widely applicable to the vast majority of magnetic bearing control problems.

References

[1] *Mu-Synthesis for Magnetic Bearings: Why Use Such a Complicated Tool?*, ser. ASME International Mechanical Engineering Congress and Exposition, vol. Volume 9: Mechanical Systems and Control, Parts A, B, and C, 11 2007. [Online]. Available: https://doi.org/10.1115/IMECE2007-43910

[2] H. Bleuler, "Decentralized control of magnetic rotor bearing systems," Ph.D. dissertation, ETH Zurich, Zürich, 1984, diss. Techn.Wiss. ETH Zürich, Nr. 7573, 0000. Ref.: Schweitzer, G. ; Korref.: Mansour, M..

[3] Q. Zhang and C.-S. Zhu, "Modal decoupling control for active magnetic bearing-supported flywheel rotor system," *Zhendong Gongcheng Xuebao/Journal of Vibration Engineering*, vol. 25, pp. 302–310, 06 2012.

[4] M. Hutterer, M. Hofer, and M. Schrödl, "Decoupled control of an active magnetic bearing system for a high gyroscopic rotor," in *2015 IEEE International Conference on Mechatronics (ICM)*, March 2015, pp. 210–215.

[5] G. Schweitzer and E. H. Maslen, *Magnetic bearings: theory, design, and application to rotating machinery*. Springer, 2010.

[6] "API Standard 617 Axial and Centrifugal Compressors and Expander-compressors," 2014.

[7] C. H. Cloud, G. Li, E. H. Maslen, L. E. Barrett, and W. C. Foiles, "Practical applications of singular value decomposition in rotordynamics," *Australian Journal of Mechanical Engineering*, vol. 2, no. 1, pp. 21–32, 2005. [Online]. Available: https://doi.org/10.1080/14484846.2005.11464477

[8] J. EDMUNDS and B. KOUVARITAKIS, "Extensions of the frame alignment technique and their use in the characteristic locus design method," *International Journal of Control*, vol. 29, no. 5, pp. 787–796, 1979. [Online]. Available: https://doi.org/10.1080/00207177908922732

[9] ISO Central Secretary, "Mechanical vibration – vibration of rotating machinery equipped with active magnetic bearings. – Part 3: Evaluation of stability margin," International Organization for Standardization, Geneva, CH, Standard, 2006. [Online]. Available: https://www.iso.org/standard/39057.html

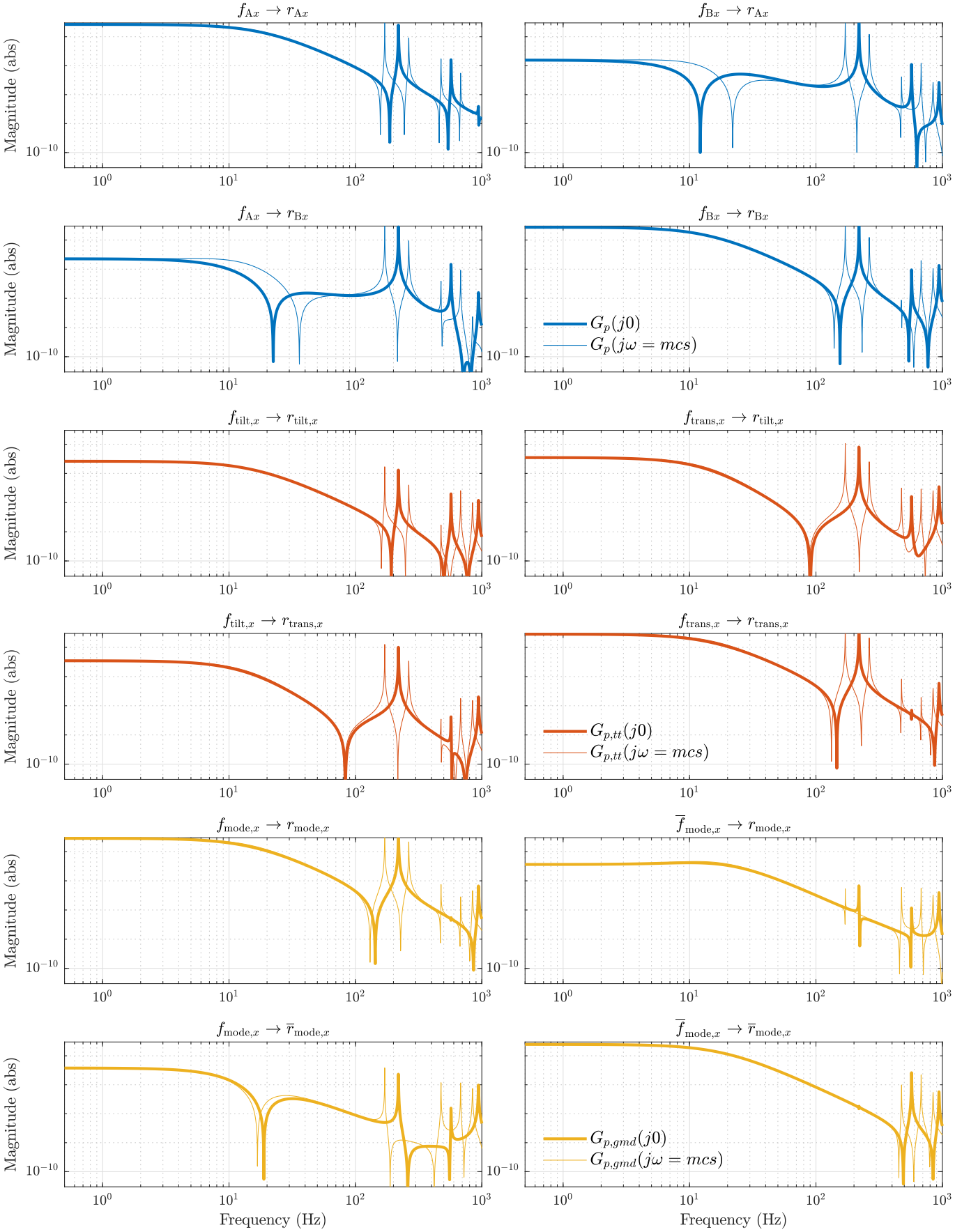

Fig. 9: Bode plot of the plant models (x-plane only). Top (blue): Initial 2x2 plant without decoupling. Middle (brown): Plant decoupled by T_{in} and T_{out} (Tilting-Translational). Bottom (gold): Plant decoupled by T_V and T_U (SVD). It is easy to see that the flexible mode is present in the main and off-diagonal channels in G_p and $G_{p,tt}$. For $G_{p,gmd}$ the mode is only present in the first channel and has a very low coupling to the other channel. The transformation has been tuned to be best at MCS for the forward mode.

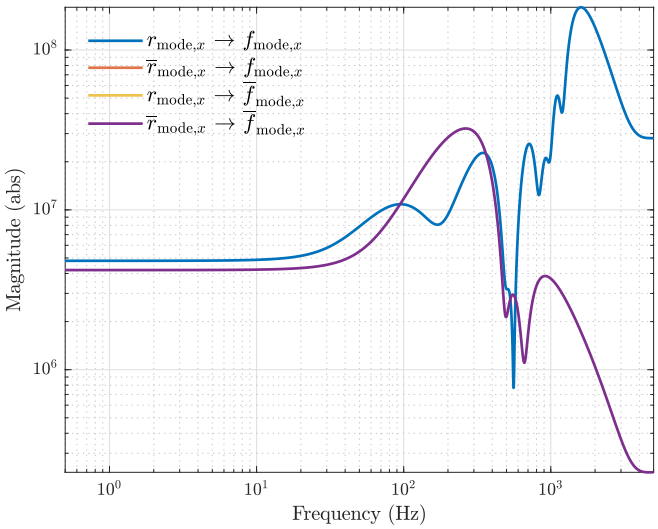

(a) Centralized controller which has no coupling between the modal decoupled channels. The controller is tuned by hand to fulfill the performance and robustness requirements for whole the speed range of the machine.

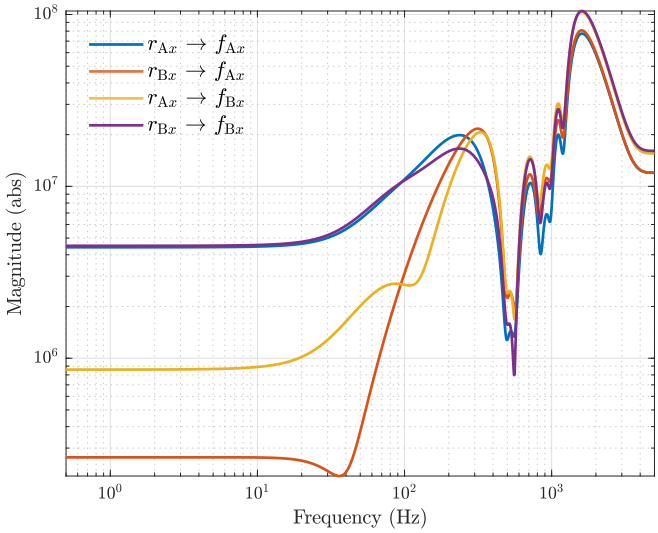

(b) Decentralized controller, generated by applying the modal decoupling T_{V} and T_{U} to the decentralized controller, showing significant and frequency dependent coupling between the sensor and actuator planes A and B.

Fig. 10: Controller in centralized (SVD) and decentralized coordinates, without integrator action. Plots are made for the x-plane. The y-plane uses the same controllers. It is worth to highlight that the controller needed to be augmented it with numerous tricks such as notch and phase bump filters to cope with spurious effects suchs as temperature depending housing resonances. Evidently, this reinforces the argument for the generalized decoupling control method as generally known methods would not provide room for corrective action, when the control design for the rotor itself is next to impossible.

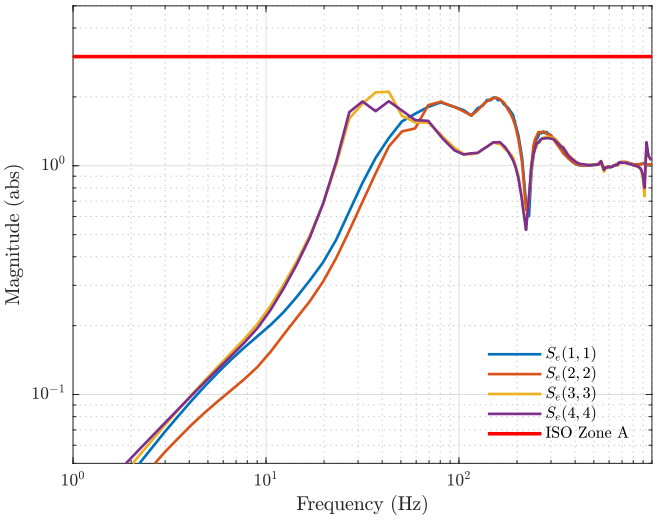

(a) Sensitivity at standstill.

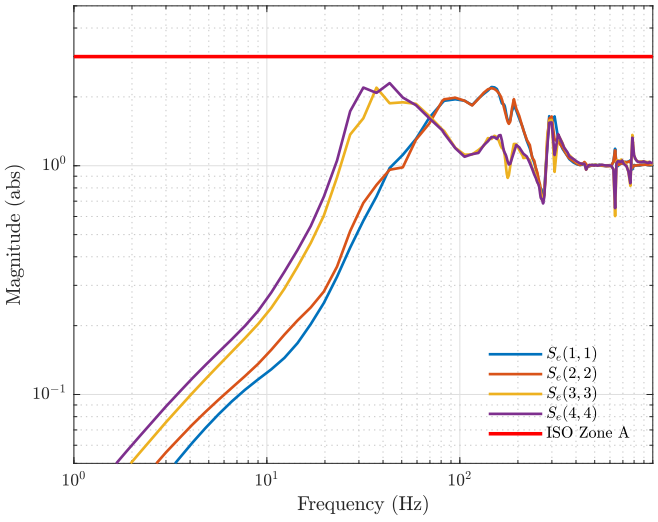

(b) Sensitivity at top speed

Fig. 11: Measured output sensitivities at standstill and top speed according to ISO [9] fall into zone A. The system features substantial robustness and excellent performance.